ELSEVIER

Colloids and Surfaces
A: Physicochemical and Engineering Aspects 198–200 (2002) 559–567

COLLOIDS AND SURFACES A

www.elsevier.com/locate/colsurfa

Synthesis of Ni-containing nanoparticles in Langmuiur–Blodgett films

G.B. Khomutov [a,*], I.V. Bykov [b], R.V. Gainutdinov [d], S.N. Polyakov [c], A.N. Sergeyev-Cherenkov [a], A.L. Tolstikhina [d]

[a] *Faculty of Physics, M.V. Lomonosov Moscow State University, Vorobjevy Gorg, 119899 Moscow, Russia.*
[b] *Vernadski Institute of Geochemistry and Analytical chemistry RAS, Moscow, Russia*
[c] *Institute of Nuclear Physics, M.V. Lomonosov Moscow State University, Moscow, Russia*
[d] *Institute of Crystallography RAS, Moscow, Russia*

Abstract

Synthesis of Ni-containing anisotropic flatten nanoparticles was carried out in a mixed Ni stearate/stearic acid and Ni arachidate/arachidic acid LB films by borohydrid reduction under different reaction conditions. The structure and composition of the films were characterized by Fourier transform infrared spectroscopy, X-ray diffraction and atomic force microscopy. Ordered lamellar structure of LB films was not disrupted by nickel reduction procedure and the presence of oblate nanoparticles was observed by AFM. © 2002 Elsevier Science B.V. All rights reserved.

Keywords: Nanoparticles; Synthesis; Langmuir–Blodgett films; Shape anisotropy; Nanotechnology; AFM; FTIR

1. Introduction

Search of effective ways for controlling the morphology of nanophase materials is of principal importance for nanotechnology and for development of advanced nano structured materials. Nanoparticles and nanoparticulate materials are a subject of growing interest from fundamental and applied viewpoints [1–6]. It is known that the method of nanoparticles synthesis often influences the properties of the product, in particularly, synthesis of nanoparticles in confined geometries and structured reaction media can result in anisotropic and size-controlled nanoparticles [7–9]. Of particular interest is the synthesis of inorganic nanoparticles in ordered organic structures, what is also the modeling of biomineralization process. In many biological systems the formation of nanocrystals occurs spontaneously and with a high degree of growth control in both shape and dimensions of the particles at highly-organized organic templates at temperatures below 100 °C and in the aqueous media. The formation of inorganic solids in biological systems is a complex and still not well-understood process. This biomineralization process has inspired the use of organic matrixes as templates for the synthesis of inorganic nanoparticles and biomimetic composite materials [10]. Thus, nucleation and controlled

* Corresponding author.
E-mail address: gbk@phys.msu.su (G.B. Khomutov).

0927-7757/02/$ - see front matter
PII: S0927-7757(01)00961-X

growth of nano sized particulates have been carried out in reverse micelles [11] and microemulsions [12], under Langmuir monolayers [13] and in self-assembled polyelectrolite films [14,15]. Supramolecular organization and structure of organic matrixes and nanoreactors can have substantial influence on the nucleation and nanoparticles growth process [10], and the use of such effects could prove to be a promising way to development of new methods for controlling the specific structure, chemical composition, crystallinity, size and shape of synthesized nanoparticles, thus opening novel possibilities for effective design of nano structured materials. Multilayer Langmuir–Blodgett (LB) films were used as a metalorganic precursor matrix and quasi-two-dimensional reaction media for the synthesis of oblate semiconductor [16–19] and metallic [20] nanoparticles. In this approach the synthesis was carried out under the gas atmosphere without liquid phase. The countercurrent diffusion method was used for the synthesis of metallic nanoparticles as interlayer within polymeric films [21]. In particularly, Ni^{2+} ions were reduced to zero-valent state with reducing agent (sodium borohydride) provided in solution [21,22].

The objectives of the present research were to investigate the features of metal clusters and nanoparticles growth in corresponding metal stearate and arachidate LB film. Such system is characterized by anisotropic confined geometry-two-dimensional (2-D) metal ion plane sandwiched in between two organic spacers. We present here our results on the generation of nickel-containing nanoparticles by borohydride reduction of Ni^{2+} in nickel stearate and arachidate multi layer LB films. The important point of such method of nanoparticles synthesis in LB films is the permanent contact of the LB film reaction media with aqueous phase what can bring substantial features in the nanoparticles growth reactions in comparison with nanoparticles synthesis in LB film matrix in a gas phase. The structure and properties of resulting material were investigated by X-ray diffraction analysis (XRD), Fourier transform infrared (FTIR) spectroscopy and atomic force microscopy (AFM). The data obtained point out to the synthesis of oblate nickel nanoparticles in Ni-containing LB films with lamellor film structure undisrupted by the presence of nanoparticles.

2. Experimental

All chemicals were purchased and used as supplied. A MilliQ water purification system was used to produce water with an average resistivity of 18 MΩ cm for all experiments.

The monolayer experiments and nickel arachidate or stearate LB films depositions were performed using Teflon Langmuir trough described elsewhere [23]. Langmuir monolayers were prepared by spreading arachidic acid (AA) or stearic acid (SA) solution in chloroform (concentration 5×10^{-4} M) onto the aqueous subphases containing 2×10^{-4} M nickel acetate $Ni(CH_3COO)_2$. The subphase pH was adjusted with 0.01 M HCl or 0.01 M KOH solutions. Ni^{2+}-containing Y-type LB films were formed by the standard vertical lifting deposition of fatty acid Langmuir monolayer from Ni acetate solution (2×10^{-4} M, pH 6.5) onto the surface of naturally oxidized silicon and mica substrates (monolayer surface pressure under deposition was 25 mN m^{-1}, substrate dipping speed was 5 mm min^{-1}). Mica substrates were freshly cleaved immediately before use. Reduction of Ni^{2+} cations in multilayer LB films to zero-valent state of nickel was carried out via incubation of LB film in sodium borohydride water/ethanol (3:1) solution (sodium borohydride concentration varied from 0.01 to 0.1 M) for 2 h at ambient temperature. The morphology of samples prepared in different series of experiments was reproducible.

X-ray scattering experiments were performed with a modified 'Rigaku D/max-RC' diffractometer (X-ray wavelength $\lambda = 1.5405$ Å (CuK_α), power of X-ray source 12 kW). The period of repetition of the periodic structure was calculated directly from the positions of Bragg reflections.

We have employed infrared absorption spectroscopy to explore the changes in the nickel stearate and arachidate LB films under Ni^{2+} reduction and formation of nanoparticles. FTIR spectra were measured using PU9800 (Philips)

FTIR spectrometer in the transmission mode. We used the Diffuse Reflectance Accessory (DRA) to eliminate the interference pattern from the two surfaces of the Si substrate. Infrared spectra from 1000 to 4000 cm^{-1} were obtained for the films deposited onto Si substrate with natural oxide layer. The final spectra of the films were obtained after the subtraction of the silicon transmittance.

AFM measurements were performed with the use of Solver P47-SPM-MDT scanning probe microscope (NT MDT Ltd, Moscow, Russia) in a tapping mode. Images were measured in air at ambient temperature (21 °C) and were stable and reproducible.

3. Results and discussion

3.1. Monolayers at the air/water interface and LB films deposition

Fig. 1 shows the compression isotherms of SA monolayer on the aqueous subphase with 2×10^{-4} M nickel acetate as a function of subphase pH value. The effect of subphase pH on the properties of SA Langmuir monolayer onto the Ni^{2+} containing subphase is readily apparent from the compression isotherms. The characteristic phase transition in SA Langmuir monolayer on a pure water subphase at pH ~ 6 and 21 °C takes place at 25 mN m^{-1} (curve 1 on Fig. 1). Close compression isotherms are known for stearic and arachidic acid monolayers on the water subphase with multivalent metal cations at low pH values when acidic carboxylic groups are protonated and metal cations do not bind and affect the monolayer [24,25]. Due to the metal cation binding with monolayer under increasing in subphase pH the fractions of free acid and soap coexist in monolayer what results in characteristic changes in monolayer compression isotherms due to phase behavior of a mixed monolayer [24–27]. At high enough pH values dependent on the metal cation nature the fatty acid monolayer is condensed and converted completely to the salt form what is manifested by characteristic compression isotherm without L_2/LS phase transition [25]. As it follows from curves 2 and 3 on Fig. 1 the fraction of Ni stearate soap in the monolayer increases with increase in pH value. The same behavior was observed with arachidic acid monolayer. The soap fraction can be estimated quantitatively using the evaluation procedure based on the analyses of compression isotherm parameters [25]. We deposited multilayer LB films at pH 6.5 at which the fraction of Ni soap in the monolayer was evaluated to be ~ 50%. Three types of samples were prepared in the series of experiments–control multilayer Ni–SA and Ni–AA LB films (sample 1), Ni–SA and Ni–AA LB films treated with diluted $NaBH_4$ solution (1×10^{-2} M, pH 6.5) (sample 2), Ni–SA and Ni–AA LB films treated with concentrated $NaBH_4$ solution (1×10^{-1} M, pH 10)(sample 3).

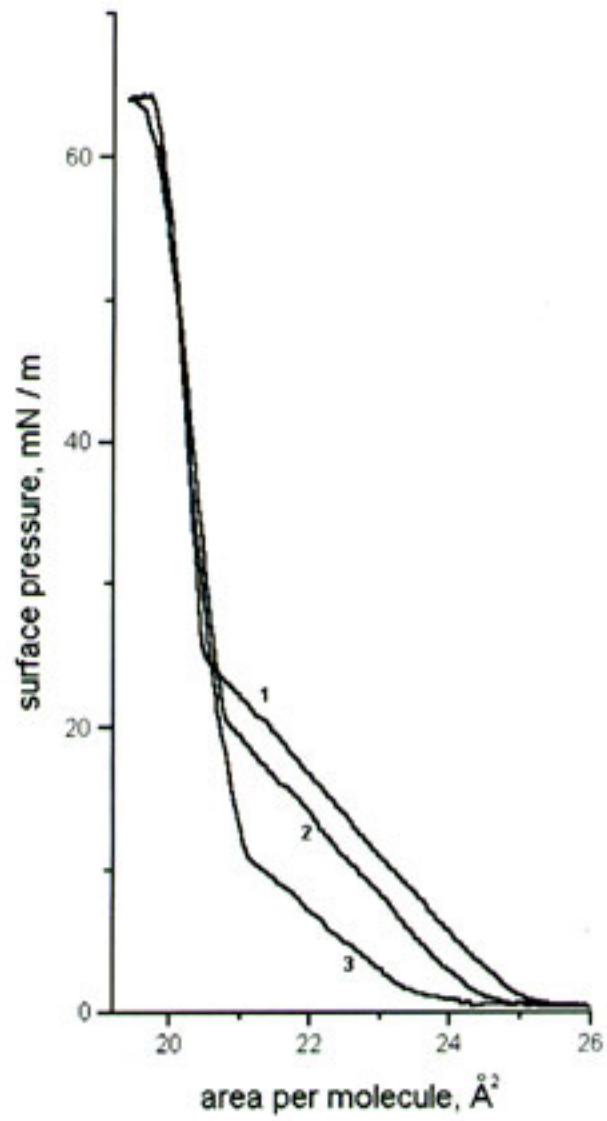

Fig. 1. Surface pressure-area isotherms obtained of stearic acid monolayer on pure water, pH 5.6 (curve 1), and on a 2×10^{-4} M $Ni(CH_3COO)_2$ solution at pH 5.8 (curve 2) and pH 6.5 (curve 3) at room (21 °C) temperature.

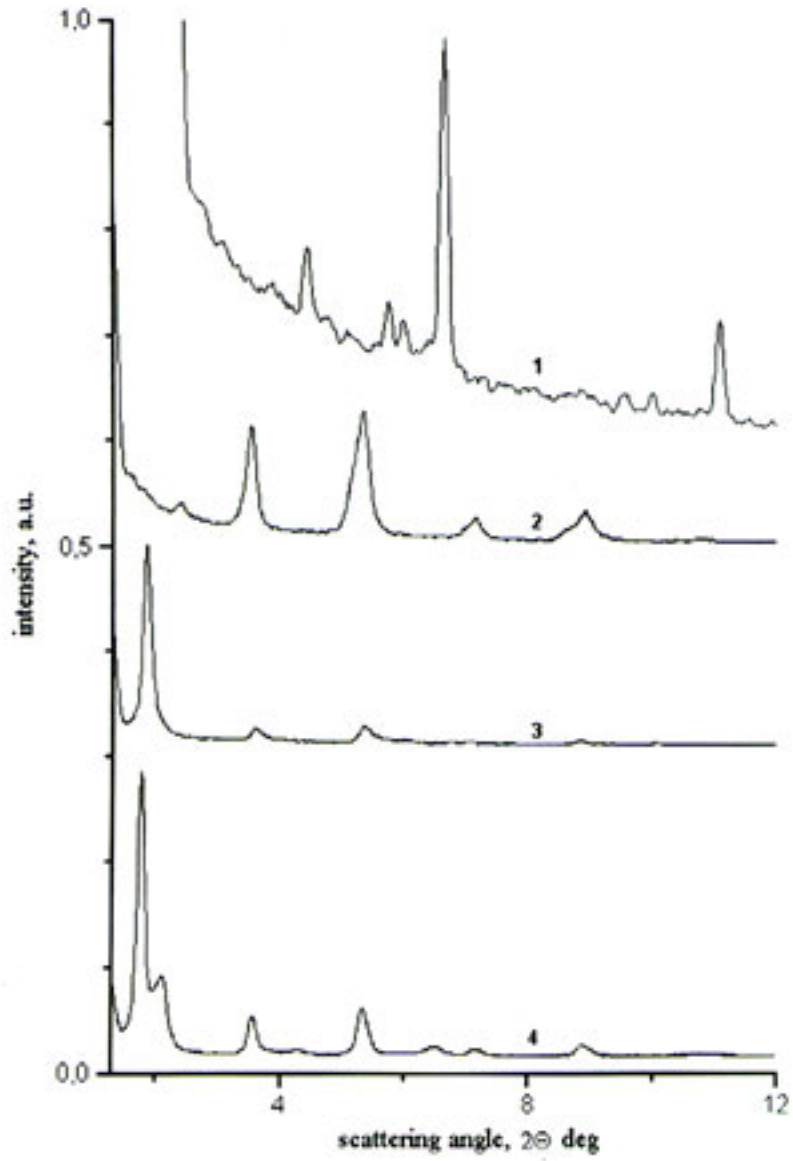

Fig. 2. X-ray reflectivity curves of multilayer LB films on silicon substrate with natural oxide layer. Curve 1–20-layer SA LB film deposited at pH 5.6; Curve 2–40 layer Ni–SA LB film deposited using 2×10^{-4} M $Ni(CH_3COO)_2$ solution at pH 6.5; Curve 3–40 layer Ni–SA LB film deposited using 2×10^{-4} M $Ni(CH_3COO)_2$ solution at pH 6.5 and treated for 2 h with $NaBH_4$ solution (1×10^{-2} M, pH 6.5); Curve 4–40 layer Ni-SA LB film deposited using 2×10^{-4} M $Ni(CH_3COO)_2$ solution at pH 6.5 and treated for 2 h with $NaBH_4$ solution (1×10^{-1} M, pH 10).

3.2. Characterization of LB films by X-ray diffractometry

X-ray measurements of all samples in θ–2θ geometry established the absence of Bragg reflections corresponding to Ni or Ni oxide phases in the 20–100° angle region. X ray analysis in the low angle range revealed the periodic well-defined layered structures characteristic for Y-type LB films shown on Fig. 2. Curve 1 on Fig. 2 represents the diffractogramm from 20-layer SA LB film recorded for monitoring the transformations in composition of Ni–SA LB films under Ni^{2+} reduction. In control sample 1 of Ni stearate LB film (Fig. 2, curve 2) X-ray measurements indicate repeat distance $d = 4.97$ nm, corresponding to the structure period of Y-type divalent metal stearates LB films [28]. The average half-maximum width of the main diffraction peaks was $W_{1/2} = 0.25°$. Using Scherrer's formula [29] the positional coherence length D value was evaluated from a full-width at a half-maximum of reflections $W_{1/2}$ to be 40 nm. Minor peaks corresponding to the low d values (at 2.35°, $d \sim 4$ nm) and unresolved shoulders (probably originated from the fraction of unionized stearic acid molecules) are also seen in the diffractogram. Curves 3 and 4 on Fig. 2 show the XRD patterns obtained from the samples 2 and 3 correspondingly (after $NaBH_4$ treatment). Ordered lamellar structure of LB films was not disrupted noticeably by the nickel reduction procedure. Narrow diffraction peaks of different orders were clearly observed in 1–10° range. It follows from the comparative analysis of diffractogramms measured for the sample 1 and samples 2 and 3 that sodium borohydrid treatment causes characteristic changes in the LB film structure. LB films with reduced Ni consist of two lamellar areas with different interlayer periods $d_1 = 4.95$ nm and $d_2 = 4.1$ nm. D values corresponding to d_1 were determined to be 55.5 nm for the sample 2 and 67.1 nm for the sample 3 indicating the ordering of LB film structure due to the $NaBH_4$ treatment. It implies that the generation of flatten Ni-containing nanoparticles can be an ordering factor (especially for sample 2), and also complete ionization of stearic acid molecules in sample 3 can further improve the film structure. The reflections corresponding to d_2 in curve 3 are of the same order of intensity as reflections corresponding to d_1. The reflections on the diffractogramms 2 and 3 are characterized by asymmetric shape (expansion to the high angle region) what can be caused by the uniform distortion of the film structure by the presence of planar nickel-containing nanoparticles shaped as ultrathin sheets with definite local order.

Ordered lamellar structure of LB films was not disrupted noticeably in our experiments by nickel

reduction procedure and the presence of nanoparticles. At the same time it is known that distortions of LB film structure can be revealed by X-ray diffraction [18,30,31]. For instance, the formation of rather thick nanoparticles with the height ($\sim$15–20 nm) exceeding the LB film bilayer structural unit, resulted in the disruption of LB film lamellar structure after the particles formation [20].

3.3. Characterization of LB films by FTJR spectroscopy

FTIR measurements were carried out with the aim to correlate the differences in structure observed between the control Ni stearate LB films and LB films after $NaBH_4$ treatment, and to obtain information about the dissociation degree of carboxilic groups in the films. FTIR spectroscopy has proven to be an effective technique for this type of study since the COOH and ionized metal-bound carboxylic groups have characteristic absorption bands in the IR region [32]. Fig. 3 shows the transmission infrared spectra of 20-layer SA LB film and of built-up 40-layer LB films on the silicon substrate. Strong asymmetric (2917 cm^{-1}) and symmetric (2849 cm^{-1}) CH_2 stretching bands and CH_3 asymmetric stretching band (2954 cm^{-1}) were observed in the transmission spectra giving evidence that hydrocarbon chains were oriented mainly perpendicular to the film plane. The absence of noticeable progression bands of methylene (–CH_2–) wagging, rocking and twisting vibrations in trans conformation with transition dipole parallel to the trans-zigzag chain axis [33,34] in the region between 1360 and 1180 cm^{-1} also support the orthogonal orientation of fatty acid molecules in built-up LB films. The frequency values of CH_2 stretching bands with a full-width at a half-maximum value of $\sim$20 cm^{-1} points out to the an all-trans conformation of the fatty acid alkyl chains and to the closely packed structure of the LB films [35,36]. A band due to a C=O stretching mode of COOH group appears at 1703cm^{-1} in spectra 1, 2 and 3. This frequency corresponds to the C=O stretching mode of carboxylic acids forming ring dimers with hydrogen-bonded carboxylic groups [37]. Such C=O stretching mode frequency was reported for arachidic [38] and stearic acid [39] multilayer LB films. When the hydrogen ion on the carboxyl group is liberated the peaks due to the asymmetric stretching vibration and symmetric stretching vibrations in the carboxylate group appear near 1550 and 1433 cm^{-1}, respectively, with the simultaneous decrease in the C=O stretching peak. The salt and acid content in the deposited LB films can be determined quantitatively from the infrared spectra by comparing the intensity of the peak at 1703 cm^{-1} with that of the CH_2 asymmetric stretching vibrations or CH wagging mode at 1467 cm^{-1} [38]. Such evalua-

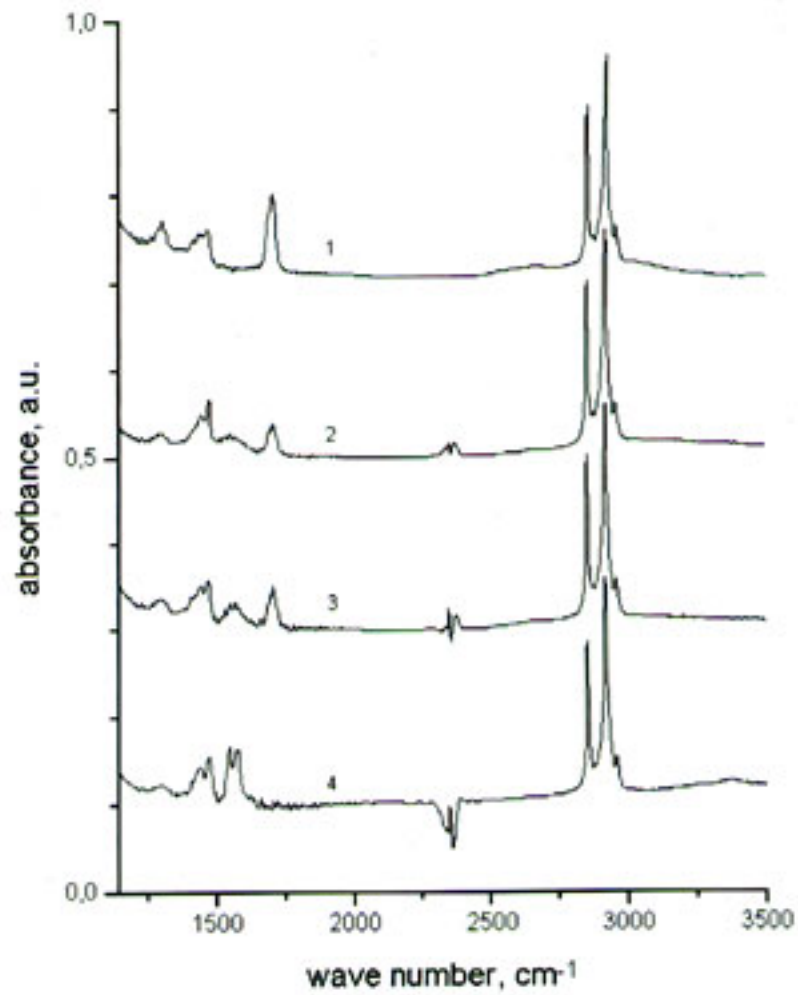

Fig. 3. FTIR transmission spectra of multilayer LB films on silicon substrate with natural oxide layer. Curve 1–20-layer SA LB film deposited at pH 5.6; Curve 2–40 layer Ni-SA LB film deposited using 2×10^{-4} M nickel acetate $Ni(CH_3COO)_2$ subphase at pH 6.5; Curve 3–40 layer Ni-SA LB film deposited using 2×10^{-4} M nickel acetate $Ni(CH_3COO)_2$ subphase at pH 6.5 after incubation for 2 h in 0.01 M sodium borohydride (pH 6.5); Curve 4–40 layer Ni-SA LB film deposited using 2×10^{-4} M nickel acetate $Ni(CH_3COO)_2$ subphase at pH 6.5 after incubation for 2 h in 0.1 M sodium borohydride solution (pH 10).

tions give a value of the Ni stearate fraction in the control LB film (curve 2) about 50%. We have studied also the changes in the sample 1 after the incubation for 2 h in the water/ethanol 3:1 mixture without sodium borohydrid, and have found some small tendency to increase the fraction of protonated carboxilic groups in LB films probably due to the Ni^{2+} leaving LB films as a result of its chemical potential gradient. Curve 3 on Fig. 3 shows the infrared spectra obtained after the incubation of control Ni stearate LB film with $NaBH_4$ (1×10^{-2} M, pH 6. 5) for 2 h at ambient temperature. One can see from the curves 2 and 3 that the intensity of the peak at 1703 cm^{-1} increased what implies the transformation of Ni stearate salt molecules into protonated acidic form under borohydrid reduction of Ni^{2+}. The presence of COO^- stretching mode vibrations in the spectrum 3 implies that not all fatty acid molecules are converted to COOH after Ni^{2+} reduction. This finding may be a result of incomplete reduction of Ni^{2+} cations under these 'soft' conditions or due to the presence of a layer of ionized fatty acid molecules on the surface of Ni containing particles. The existence of such capping layers of ionized arachidic acid molecules on the surface of CdS particles synthesized in cadmium arachidate LB films by exposure to H_2S was proposed in [19]. The ionic nature of the fatty acid interaction with α-Fe_2O_3 nanoparticles in nanoparticulate SA LB films was reported in [40] and may be relevant for the SA LB films with formed Ni-containing nanoparticles which can be at least partially oxidized under air conditions. Spectrum 4 was obtained after the treatment of Ni stearate LB film for 2 h in a concentrated $NaBH_4$ solution (1×10^{-1} M, pH 10, ambient temperature). We have observed that no C=O stretching band remained at 1703 cm^{-1} and all COOH groups were ionized after such treatment. This finding is in agreement with data of [41] that under high pH values SA LB films are completely ionized. A broad peak near 3400 cm^{-1} due to OH stretching and HOH bending modes [42] is also present in spectrum 4 indicating that the films contain water molecules and/or OH-coordinated to the metal ion or Ni hydroxide nanoparticles were formed.

3.4. Characterization of LB films by AFM

Fig. 4 shows the AFM tapping mode topographic images of Ni-AA LB film deposited on the mica substrate after one cycle of vertical substrate lifting. One can see macroscopically flat structure with small number of objects of ~ 5 nm size, which can be structural defects and 3-D aggregates. Typical height cross section of image (b) is shown in picture (d) and indicates an overall film roughness of ~ 3 nm, corresponding to the monolayer of AA molecules. AFM topographic image of the same sample as on Fig. 4 but after 2 h incubation in a concentrated $NaBH_4$ solution (1×10^{-1} M, pH 10, ambient temperature) is shown on Fig. 5. It follows from Fig. 5 that morphology of Ni–AA LB film was changed substantially after such treatment. Large plateaus of ~ 6 nm height (corresponding to AA bilayers) and ~ 500 nm diameter with nanoparticles are seen in the Fig. 5.

The height histogram on Fig. 5(d) with two broad peaks corresponding to most frequently present structure heights with main height difference 7 nm clearly indicates to the terrace structure of the film with main nanoparticle height about of 7 nm (main diameter 40 nm can be evaluated from the images (a) and (b)). AFM study of Ni–AA LB film after treatment with diluted $NaBH_4$ solution (1×10^{-2} M, pH 6.5) did not reveal noticeable morphological changes due to nanoparticles formation.

Our results are in agreement with known data on the synthesis of inorganic nanoparticles in multilayer LB films. Generally, the formation of oblate nanoparticles was reported. Relatively thick metallic gold nanoparticles were photochemically generated in multilayer LB films of positively charged amphiphiles deposited from an aqueous $HAuCl_4$ subphase (diameter ranged from 20 to 800 nm and height 15–20 nm, lamellar structure of LB films was disrupted after the particles formation) [20]. The formation of semiconductor CdS nanoparticles via Cd soap LB films exposure to H_2S also resulted in generation of flatten CdS clusters [9]. The morphology of CdS particles was dependent on the LB film matrix. Thus, the generation of ultraflat CdS parti-

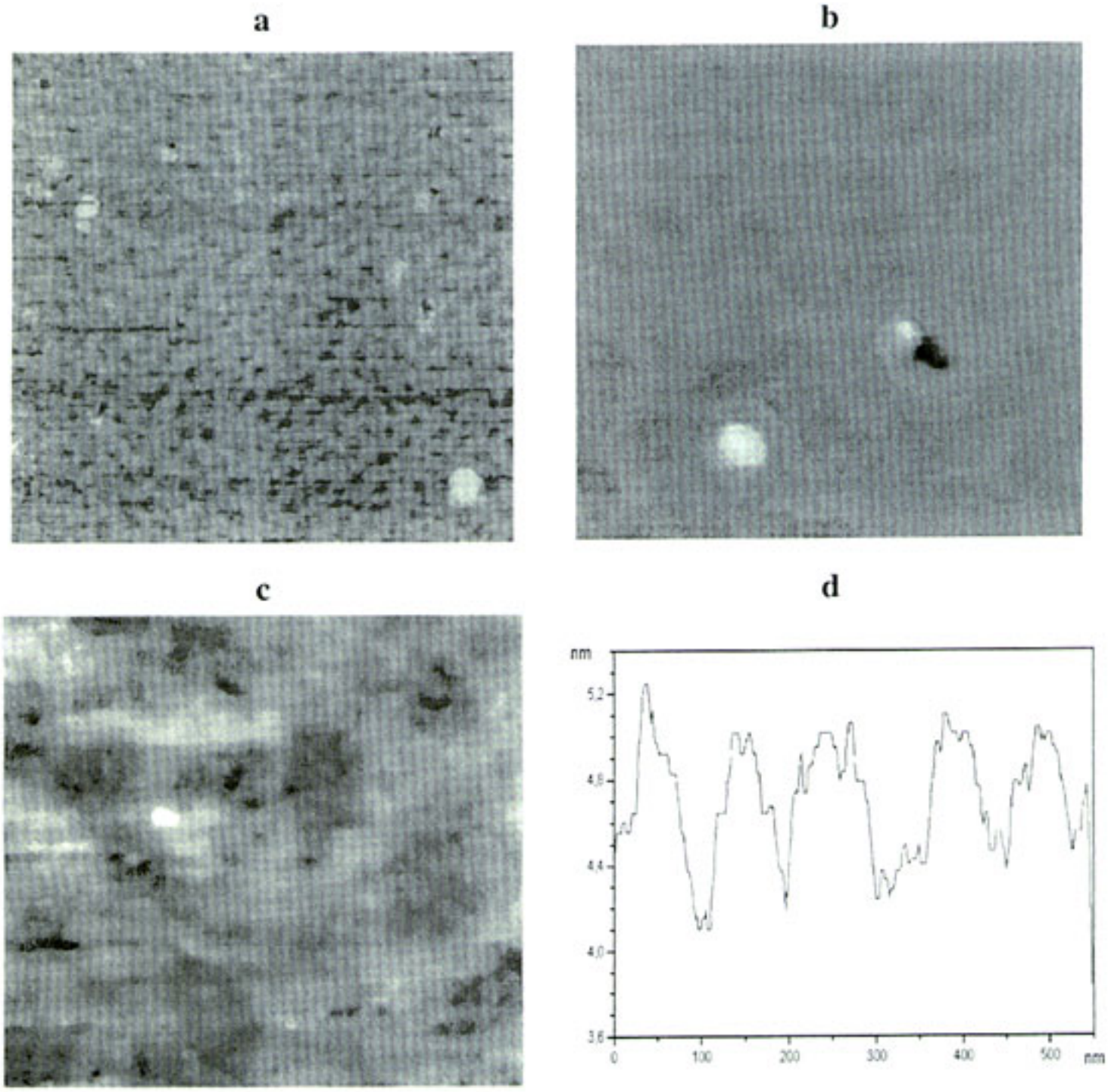

Fig. 4. AFM tapping mode topographic images of bilayer Ni-AA LB film deposited on the mica substrate by the vertical substrate lifting. (a), (b) and (c)-AFM top view images 2.2×2.2 μm (black-to-white vertical color scale is 1.8–4.4 nm), 550×550 nm (black-to-white vertical color scale is 0–10 nm) and 220×220 nm (black-to-white vertical color scale is 0–1.625 nm), correspondingly. (d)-Typical height cross section of image (b).

cles in calixarene LB films (where diffusion of CdS molecules (and, possibly, H_2S) within the layers of LB film matrix was slowed down) did not affect substantially their layered structure, in contrast cadmium stearate LB films were substantially destroyed by formation of much larger CdS clusters [18,30]. These results give evidence that the slowing down of two-dimensional nanoparticle growth rate results in the formation of more flatten nanoparticles. Mixed Ni soap/fatty acid LB films used in our experiments as precursors for nanoparticles synthesis and diluted reducing $NaBH_4$ solution (1×10^{-2} M, pH 6.5) possibly resulted in reduction the nanoparticle growth rate with generation of rather flatten nanoparticles. The oblate structure of nanoparticles synthesized in LB films can be result of quasi-two-dimensional nature of LB film templates and mainly 2-D character of diffusion of active intermediates in the layers of amphiphile molecules.

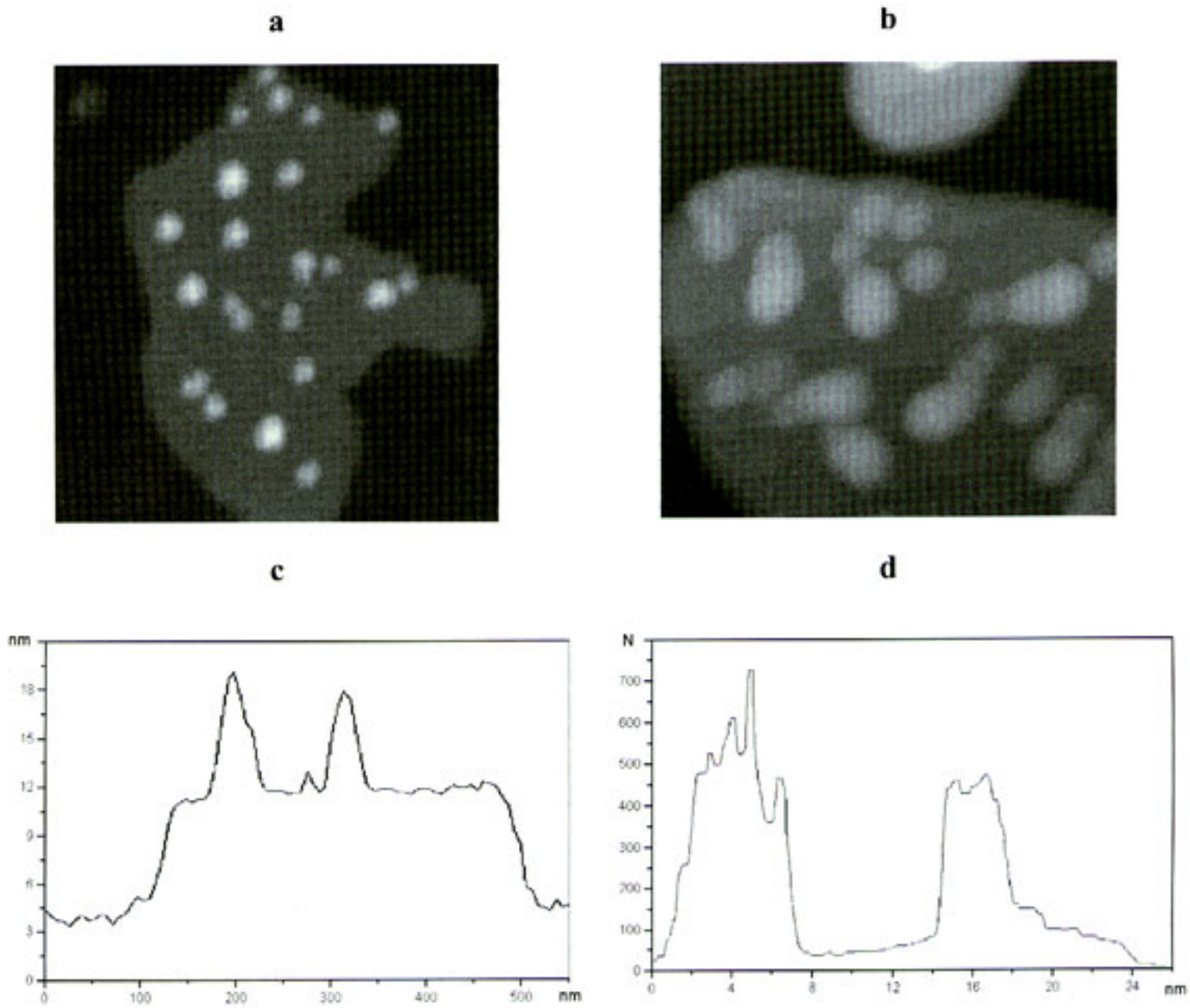

Fig. 5. AFM tapping mode topographic images of Ni-AA LB film deposited on the mica substrate by the vertical substrate lifting after 2 h incubation in $NaBH_4$ solution (1×10^{-1} M, pH 10, 21 °C). (a) and (b)-AFM top view images 550 × 550 nm (black-to-white vertical color scale is 0–30 nm) and 280 × 280 nm (black-to-white vertical color scale is 0–20 nm), correspondingly. (c)-typical height cross section of image (a). (d)-height histogram of the image (b).

4. Conclusions

We demonstrate the generation of Ni-containing anisotropic plate-like nanoparticles in the mixed Ni stearate/stearic acid and Ni arachidate/arachidic acid LB films by borohydrid reduction. Ordered lamellar structure of LB films was not disrupted by the nickel reduction procedure and presence of oblate nanoparticles. Nanoparticles were directly observed by AFM. The oblate shape of obtained nanoparticles can reflect the layered nature of LB film templates where important features are quasi-two-dimensional character of reaction area and mainly planar diffusion of active intermediates parallel to the surfactant layers resulting in the quasi-two-dimensional growth of flat nanoparticles.

Acknowledgements

This work was supported by Russian Foundation for Basic Researches (Grant 99-03-32218).

References

[1] Yu.A. Petrov, Clusters and Small Particles, Nauka, Moscow, 1986.
[2] G. Schmid (Ed.), Clusters and Colloids. From theory to Applications, VCH, Weinheim, 1994.
[3] U. Kreibig, M. Vollmer (Eds.), Optical Properties of Metal Clusters, Springer, New York, 1995.
[4] J.H. Fendler, I. Dekany (Eds.), Nanoparticles in Solids and Solutions, Kluwer Academic Publishers, Dordrecht, 1996.
[5] A.P. Alivisatos, Science 271 (1996) 933.
[6] C.P. Collier, R.J. Saykally, J.J. Shiang, S.E. Henrichs, J.R. Heath, Science 277 (1997) 1978.
[7] C.K. Preston, M. Moskovits, J. Phys. Chem. 97 (1993) 8495.
[8] D. AlMawlawi, N. Coombs, M. Moskovits, J. Appl. Phys. 70 (1991) 4421.
[9] G.B. Khomutov, A.Yu. Obydenov, S.A. Yakoveriko, E.S. Soldatov, A.S. Trifonov, V.V. Khanin, S.P. Gubin, Mat. Sci. Eng. C 8–9 (1999) 309.
[10] S. Mann, D.D. Archibald, J.M. Didymus, T. Douglas, B.R. Heywood, F.C. Meldrum, N.J. Reeves, Science 261 (1993) 1286.
[11] Y.Y. Yu, S.S. Chang, C.L. Lee, C.R.C. Wang, J. Phys. Chem. B 101 (1997) 6661.
[12] J.H. Fendler, Chem. Rev. 87 (1987) 877.
[13] K.C. Yi, V.5. Mendieta, R.L. Castanares, F.C. Meldrum, C. Wu, J.H. Fendler, J. Phys. Chem. 99 (1995) 9869.
[14] S. Dante, Z. Hou, S. Risbud, P. Stroeve, Langmuir 15 (1999) 2177.
[15] S. Joly, R. Kane, L. Radzilowski, T. Wang, A. Wu, R.E. Cohen, E.L. Thomas, M.F. Rubner, Langmuir 16 (2000) 1354.
[16] E.S. Smotkin, C. Lee, A.J. Bard, A. Campion, M.A. Fox, T.E. Mallouk, S.E. Webber, J.M. White, Chem. Phys. Lett. 152 (1988) 265–268.
[17] V. Erokhin, L. Feigin, G. Ivakin, V. Klechkovskaya, Y.u. Lvov, N. Stiopina, Macromol. Chem. Macromol. Symp. 46 (1991) 359.
[18] A.V. Nabok, A.K. Ray, A.K. Hassan, J.M. Titchmarsh, F. Davis, T. Richardson, A. Starovoitov, S. Bayliss, Mat. Sci. Eng. C 89 (1999) 171.
[19] R.S. Urquhart, C.L. Hoffmann, D.N. Furlong, N.J. Geddes, J.F. Rabolt, G. Franz, J. Phys. Chem. 99 (1995) 15987.
[20] S. Ravaine, G.E. Fanucci, C.T. Seip, J.H. Adair, D.R. Talham, Langmuir 14 (1998) 708.
[21] L.E. Manring, S. Mazur, US Patent 4,692,360, (1987).
[22] S.V. Stakhanova, E.S. Trofimchuk, N.I. Nikonorova, A.V. Rebrov, A.N. Ozerin, A.L. Volynskii, N.F. Bakeev, Polymer Sci. A 39 (1997) 229.
[23] G.B. Khomutov, S.A. Yakovenko, E.S. Soldatov, V.V. Khanin, M.D. Nedelcheva, T.V. Yurova, Membr. Cell Biol. 10 (1997) 665.
[24] J.A. Spink, J.V. Sanders, Trans. Faraday Soc. 51 (1955) 1154.
[25] M.L. Kurnaz, D.K. Schwartz, J. Phys. Chem. 100 (1996) 11113.
[26] J.A. Spink, J. Coll. Interf. Sci. 23 (1967) 9.
[27] H. Reigler, K. Spratte, Thin Solid Films. 210–211 (1992) 9.
[28] G.L. Gaines, Insoluble Monolayers at Liquid–Gas Interfaces, Willey, New York, 1966.
[29] A. Guinier, X-ray Diffraction, Freeman, San Francisco, 1963.
[30] A.V. Nabok, T. Richardson, C. McCartney, N. Cowlam, F. Davis, C.J.M. Stirling, A.K. Ray, V. Gacem, A. Gibaud, Thin Solid Films 327-329 (1998) 510.
[31] G.B. Khomutov, A.M. Tishin, S.N. Polyakov, J. Bohr, Coll. Surf. A 166 (2000) 33.
[32] G. Roberts, Langmuir–Blodgett Films, Plenum, New York, NY, 1990.
[33] R.G. Snyder, J. Mol. Spectrosc. 4 (1960) 411.
[34] R.G. Snyder, J.H. Schachtschneider, Spectrochim. Acta 19 (1963) 85.
[35] R. Maoz, J. Sagiv, J. Coll. Interf. Sci. 100 (1984) 465.
[36] T. Sato, Y. Ozaki, K. Inyama, Langmuir 10 (1994) 2363.
[37] S.N. Vinogradov, R.H. Linnell, Hydrogen Bonding, Reinhold, New York, 1971.
[38] D.J. Johnson, D.T. Amm, T. Laursen, S.K. Gupta, Thin Solid Films 232 (1993) 245.
[39] M. Linden, J.B. Rosenholm, Langmuir 11 (1995) 4499.
[40] J. Yang, X.G. Peng, Y. Zhang, H. Wang, T.-J. Li, J. Phys. Chem. 97 (1993) 4484.
[41] C. Vogel, J. Corset, M. Dupeyrat, J. Chim. Phys. 76 (1979) 909.
[42] K. Nakamato, Infrared and Raman Spectra of Inorganic and Coordination Compounds, Fourth ed., Wiley, New York, 1986, p. 232.